JACS
JOURNAL OF THE AMERICAN CHEMICAL SOCIETY
Cite This: J. Am. Chem. Soc. 2018, 140, 11594−11598
Communication
pubs.acs.org/JACS

Edge-Site Engineering of Atomically Dispersed Fe−N_4 by Selective C−N Bond Cleavage for Enhanced Oxygen Reduction Reaction Activities

Rui Jiang,[†] Li Li,[†] Tian Sheng,[‡] Gaofei Hu,[†] Yueguang Chen,*[,†] and Leyu Wang*[,†]

[†]State Key Laboratory of Chemical Resource Engineering, Beijing Advanced Innovation Center for Soft Matter Science and Engineering, Beijing University of Chemical Technology, Beijing 100029, China

[‡]College of Chemistry and Materials Science, Anhui Normal University, Wuhu 241000, China

Supporting Information

ABSTRACT: Single-atom metal−nitrogen−carbon (M−N−C) catalysts have sparked intense interests, but the catalytic contribution of N-bonding environment neighboring M−N_4 sites lacks attention. Herein, a series of Fe−N−C nanoarchitectures have been prepared, which confer adjustable numbers of atomically dispersed Fe−N_4 sites, tunable hierarchical micro-mesoporous structures and intensified exposure of interior active sites. The optimization between Fe−N_4 single sites and carbon matrix delivers superior oxygen reduction reaction activity (half-wave potential of 0.915 V vs RHE in alkaline medium) with remarkable stability and high atom-utilization efficiency (almost 10-fold enhancement). Both experiments and theoretical calculations verified the selective C−N bond cleavage adjacent to Fe center induced by porosity engineering could form edge-hosted Fe−N_4 moieties, and therefore lower the overall oxygen reduction reaction barriers comparing to intact atomic configuration. These findings provide a new pathway for the integrated engineering of geometric and electronic structures of single-atom materials to improve their catalytic performance.

With increasing energy demands and environmental pollution issues, fuel cells have arisen as one of the most promising devices to provide sustainable, clean energy conversion pathways.[1−3] The pivotal process is oxygen reduction reaction (ORR),[4] a kinetically sluggish process that basically relies on expensive Pt-based catalysts.[5−10] Recently, metal−nitrogen−carbon (M−N−C, M refers to nonprecious Fe, Co etc.) materials, using N to anchor dispersed metal atoms, are burgeoning alternatives due to their unique electronic properties and high atom-utilization efficiency.[11−18] Despite extensive efforts, further enhancing the performance of M−N−C materials possesses massive uncertainties, mainly for two reasons. First, a synthetic method lacks the accurate atomic control of metals, typically resulting in multispecies (metallics, oxides) and ambiguous molecular geometries.[19,20] Fabricating monodispersed metal sites with sufficient availability is still challenging. Second, both the downsized M−N_x architectures and the macrostructures of the whole catalyst are crucial design criteria that determine the overall efficiency.[21−23] Unfortunately, establishing their synergistic correlation to manifest the structure−activity relationship is highly appealing yet difficult. Particularly, although many efforts have been made to identify the coordination structure of metal centers,[4,24,25] attention has rarely been paid to the effects of N−C bonding environment in single-atom materials.

Herein, we prepared atomically dispersed Fe−N_4 sites anchored on three-dimensional (3D) hierarchically porous carbon by precisely atomic-level control, which possessed well-defined single-atom sites (SAs), adjustable mass loadings and enhanced active-site accessibility. Even with 0.20 wt % of nonprecious metal, Fe SAs-N/C-20 catalyst exhibits superior ORR performance with a half-wave potential ($E_{1/2}$) of 0.915 V (vs RHE) in 0.1 M KOH, higher than that of commercial Pt/C ($E_{1/2}$ = 0.85 V) and most M−N−C catalysts. Remarkably, the atom-utilization efficiency outperformed most previous reports, up to 10-fold enhancement. On the basis of experiments and density functional theory (DFT) results, we found hierarchical carbon pores successfully optimized the electronic structure of Fe−N_4 by changing the local coordination of pyridine-like N, which enables the selective C−N bond cleavage (SBC) adjacent to Fe centers to form edge-hosted Fe−N_4 moieties, and therefore lowers the overall ORR barriers to acquire excellent activity and long-term durability.

As presented in Figure 1a, iron (II) phthalocyanine (FePc) molecules were first encapsulated into cavities of zeolitic imidazolate framework (ZIF) during the assembly of Zn^{2+} and 2-methylimidazole (MeIM) to form FePc-*x*@ZIF-8 nanocomposites (*x* refers to the addition of FePc and *x* = 8, 16, 20, 24 mg, respectively; Figure 1b, Figure S1, ZIF-8 shown in Figure S2). FePc (molecular size, 14.6 Å) bursted the ZIF cage (cavity diameter, 11.6 Å) to break the confinement effect of microcavity (Figure S3), which played a crucial role in the edge-site engineering and mesopore construction. The subsequent pyrolysis was carefully optimized to guarantee that ZIF-8 evolved into 3D N-doped carbon (Figures S4 and S5),[18,26] while single FePc molecule trapped within broken cavities was reduced *in situ* to form edge-hosted, atomically dispersed Fe−N site.[27] Simultaneously, excessive FePc multimolecular aggregates would induce the generation of Fe_2O_3 and enlarged mesopores through the Kirkendall effect (Figures

Received: July 19, 2018
Published: August 31, 2018

DOI: 10.1021/jacs.8b07294
J. Am. Chem. Soc. 2018, 140, 11594−11598

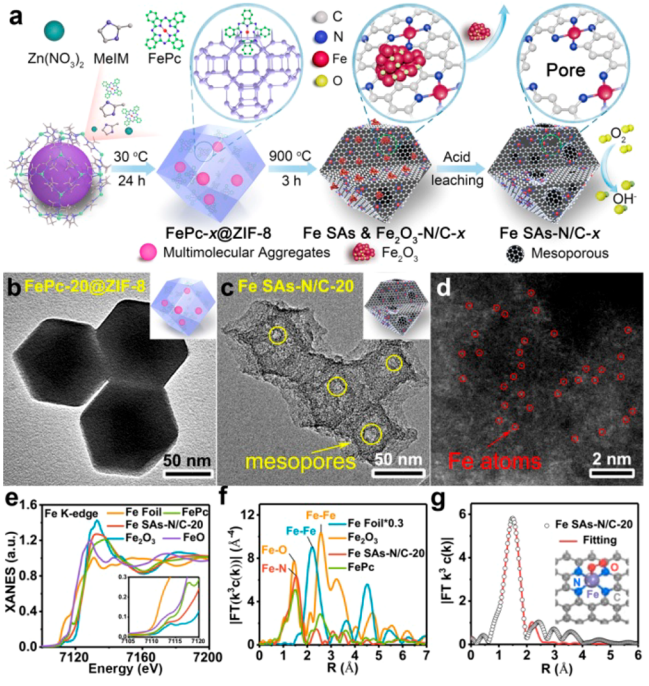

Figure 1. (a) Schematic illustration. (b) TEM image of FePc-20@ZIF-8 composite. (c) HRTEM, (d) HAADF-STEM of Fe SAs-N/C-20 catalyst. (e) Fe K-edge XANES (inset is the magnified image) and (f) FT k^3-weighted EXAFS spectra of Fe SAs-N/C-20 and the reference samples. (g) Corresponding FT-EXAFS fitting curves of Fe SAs-N/C-20.

S6 and S7).[28] Finally, acid-leaching removed extra metal species in Fe SAs and Fe_2O_3−N/C-*x* hybrid nanostructures to obtain hierarchically porous Fe SAs-N/C-*x* catalysts (Figure 1c).[29]

The aberration-corrected high-angle annular dark-field scanning transmission electron microscopy (AC HAADF-STEM) images of Fe SAs-N/C-20 revealed that individual Fe atoms were homogeneously dispersed throughout the porous carbon (Figure 1d, Figure S8). X-ray diffraction (XRD) patterns for Fe SAs-N/C-*x* samples displayed two broad peaks at 25° and 43° (Figure S9), which were related to the (002) and (101) planes of graphitic carbon.[30] No peaks of impurities, also corresponding to Raman spectra (Figure S10).[31] The energy-dispersive X-ray spectroscopy (EDS) analysis confirmed the uniform distribution of C, N and Fe (Figures S11 and S12).

To unravel the chemical state and coordination environment of Fe center, we performed X-ray absorption spectroscopy analysis. The Fe K-edge X-ray absorption near edge structure (XANES) spectra (Figure 1e) suggested the valence state of Fe in Fe SAs-N/C-20 was between the Fe(II) and Fe(III) states. The Fourier-transformed (FT) k^3-weighted extended X-ray absorption fine structure (EXAFS) spectra (Figure 1f, Figure S13) show that Fe SAs-N/C-20 only exhibited a prominent peak at 1.5 Å, which was mainly attributed to the Fe−N/C first coordination shell.[24,25] The structural parameters by EXAFS fitting indicated that one Fe atom was coordinated by four N atoms at 1.96 Å forming a Fe−N_4 moiety (Figure 1g, Table S1).[32,33]

Interestingly, FePc was carefully chosen as the metal−nitrogen dual precursor (Figure S14). It not only created adjustable densities of metal sites but also modulated the carbon pore size. By increasing the addition of FePc, Fe content in Fe SAs-N/C-*x* (*x* = 8, 16, 20, 24 mg) was 0.05, 0.15, 0.20, 0.24 wt %, respectively (Table S2); interior cavities began to form inside the initial carbon matrix and gradually enlarged (Figure 2a−h, Figure S15). N_2 adsorption/desorption

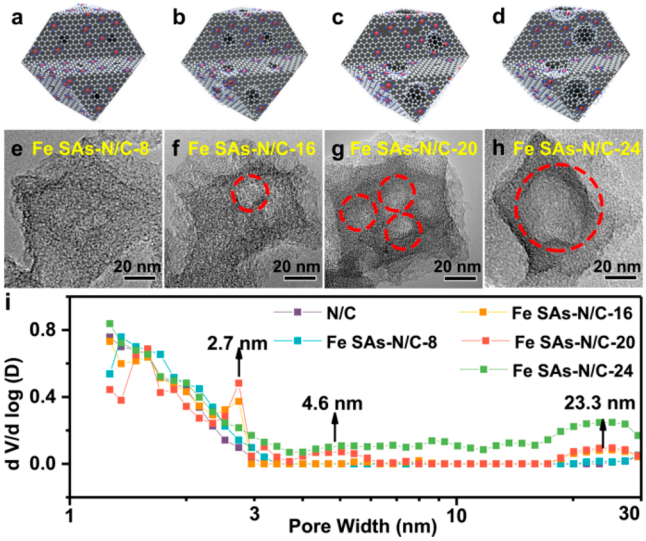

Figure 2. Schematic and TEM images of (a, e) Fe SAs-N/C-8, (b, f) Fe SAs-N/C-16, (c, g) Fe SAs-N/C-20 and (d, h) Fe SAs-N/C-24 (mesopores were highlighted by red circles). (i) DFT pore size distributions of Fe SAs-N/C-*x* (*x* = 0−24).

isotherms (Figure S16) and pore diameter distributions (Figure 2i) confirmed the existence of hierarchical micro-mesopores in Fe SAs-N/C-*x*. The original N/C had a predominantly microporous character with pore size distribution mainly below 3 nm, whereas the secondary mesopores (pore width >2 nm) developed in Fe SAs-N/C-*x* with pore size shifting from 2.7 to 23.3 nm, accompanied by the increasing pore volumes and Brunauer−Emmett−Teller (BET) surface areas (Figure S16).

The compositions of C and N were obtained by X-ray photoelectron spectroscopy (XPS) (Figure S17). Carbon species in Fe-SAs-N/C-*x* could be deconvoluted into three types:[34] C—C (284.7 eV), C—N (285.6 eV), C═O (288.2 eV) (Figure S18). Meanwhile, the high-resolution N 1s peaks were fitted into pyridinic N (398.5 eV), pyrrolic N (400.0 eV) and graphitic N (401.3 eV) (Figure S19).[35] Specifically, C—N content (Figure S18f) and pyridinic N content (Figure S19f) both showed a downward trend with the pore size expansion (Figure 3a). Thus, the enhanced porosity might trigger the selective C—N bond cleavage (SBC), preferentially coordinated to pyridinic N.

Furthermore, we used ^{13}C solid state nuclear magnetic resonance (ssNMR) to gain insights into chemical bonding network of porous carbon. The ^{13}C-ssNMR spectrum (Figure 3b) of pristine N/C showed a broad peak at δ = 100−170 ppm, the typical signal for sp^2-hybridized carbons in a graphitic-like structure. In contrast, *N*-alkyl carbons (C1 at 45.6 ppm and C2 at 53.9 ppm) of Fe SAs-N/C-*x* began to appear, which were ascribed to the cleavage of C═N structures in graphitic N and pyridinic N (cleavage process is shown in Figure S20). When the cracking degree increased from Fe SAs-N/C-16 to Fe SAs-N/C-24, further cleavage of C—N bonds intensified the signals at 10−30 ppm for sp^3-

DOI: 10.1021/jacs.8b07294
J. Am. Chem. Soc. 2018, 140, 11594−11598

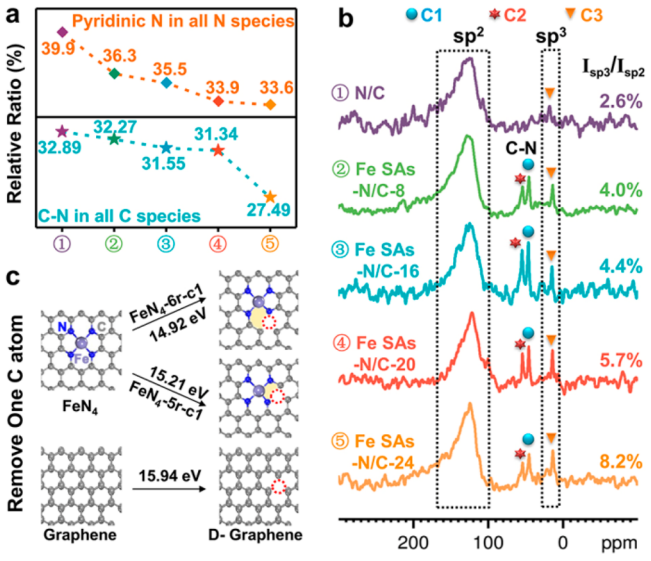

Figure 3. (a) Relative content of C—N species and pyridinic N determined by XPS analysis. (b) ^{13}C-ssNMR spectra of Fe SAs-N/C-*x* catalysts (C1 and C2 refer to two different types of *N*-alkyl carbons, C3 refers to sp^3-hybridized carbons). (c) DFT calculated formation energies for carbon vacancy (highlighted by red circles). The models are defective Fe—N_4—C (FeN_4-6r-c1 and FeN_4-5r-c1) and defective graphene (D-graphene), respectively (6r or 5r refers to six- or five-membered heterocycle ring, c1 refers to the cleavage of one C—N bond adjacent to Fe—N_4 site).

hybridized carbons (donated as C3), which in turn weakened the resonances of *N*-alkyl carbons. Notably, the peak intensity at 53.9 ppm (C2) decreased more significantly than that at 45.6 ppm (C1) (Figure 3b, Table S3), indicating the preferential cleavage of C2—N bond (adjacent to pyridinic N). From N/C to Fe SAs-N/C-24, the integrated intensity ratios of sp^3- to sp^2-hybridized carbons (I_{sp3}/I_{sp2}) grew continuously from 2.6%, 4.0%, 4.4%, 5.7% to 8.2%, which demonstrated that the selective cleavage of C—N bonds (SBC) occurred throughout the overall pore-enlarging process, coincided with XPS (Figure 3a) and C/N K-edge XANES (Figure S21) results.

In addition, we carried out DFT calculations to acquire the possible configurations of defective Fe—N_4—C. The formation energy of defective FeN_4-6r-c1 and FeN_4-5r-c1 was 14.92 and 15.21 eV (Figure 3c, details in Figure S22), respectively, lower than that of defective graphene. The C—N bond (pyridinic N attached to Fe) in six-membered Fe, N-containing heterocycle is more vulnerable, which implies that Fe—N_4 moiety with edge-N is thermodynamically favorable. Combining structural characterization and theoretical investigation, we conclude that the selective C—N bond cleavage (SBC) tailors the coordination environment of pyridinic N to achieve edge-site engineering of Fe—N_4 moieties.

The ORR performances of Fe-SAs-N/C-*x* catalysts and reference samples, including N/C and commercial Pt/C, were evaluated using the rotating disk electrode (RDE) method in O_2-saturated 0.1 M KOH solution. As shown in the linear sweep voltammetry (LSV) results (Figure 4a), Fe SAs-N/C-20 (0.20 wt % Fe) reached the highest ORR activity with half-wave potential ($E_{1/2}$) of 0.909 V (vs RHE), 59 mV more positive than that of commercial Pt/C ($E_{1/2}$ = 0.85 V) (Figure 4b, Figure S23 and Table S4) and superior to that of most non-noble-metal electrocatalysts (Table S5). It is noteworthy

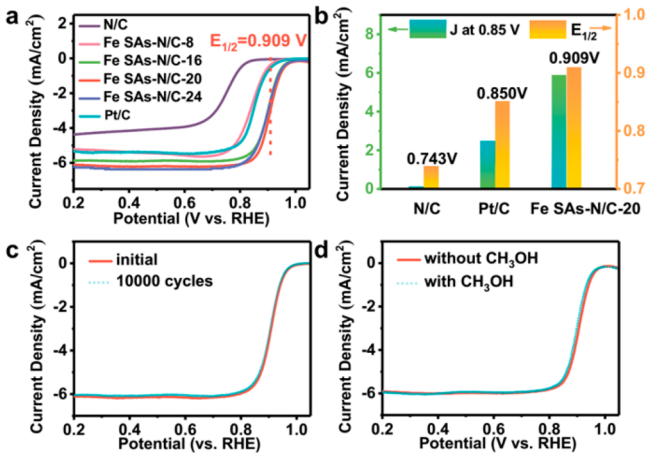

Figure 4. (a) LSV curves of Fe SAs-N/C-*x*. (b) Comparison of J and $E_{1/2}$ for different catalysts. LSV curves of Fe SAs-N/C-20 (e) before and after 10 000 successive cycles, (f) without and with 1.0 M CH_3OH. Catalyst loading: 0.408 mg cm^{-2}.

that, even in thicker electrodes, $E_{1/2}$ was further improved to 0.915 V when the catalyst loading was 0.612 mg cm^{-2} (Figure S24). The interconnected porous network delivers extremely high metal utilization efficiency and fast mass transport without ion diffusion limitations.[36] The significant enhancement in metal-utilization efficiency (almost 10 times higher than those of previous reports, Table S5) will provide an innovative way for the design of noble metal catalysts. Moreover, with a dominant four-electron ORR pathway (Figure S25),[37−39] Fe SAs-N/C-20 also showed remarkable durability (Figure 4c) and negligible fuel-crossover effect (Figure 4d). The $E_{1/2}$ of Fe SAs-N/C-24 was slightly inferior to that of Fe SAs-N/C-20, which could be ascribed to the buried active sites caused by nanostructure collapse (Figure 2h). Overall, the excellent activity and promoted accessibility to interior active sites synergistically motivated outstanding ORR performance, making the hierarchical porous Fe—N—C highly promising materials for next-generation energy.

To reveal intrinsic properties of edge-hosted Fe—N_4 moieties, five Fe—N_4/C models with different edge-N atoms were proposed by DFT investigations (Figure 5a, details in Figure S26). At the equilibrium potential U = −0.77 V (vs SHE) (Figure 5b and Table S6), the four-electron reduction pathways have negative values for the free energy change (ΔG), and thus are exothermic. However, at U = 0.13 V (vs SHE), the largest positive ΔG from the first electron transfer substep ($*O_2 + H_2O + e^- \rightarrow *OOH + OH^-$) demonstrates the sluggish rate-determining step. Among the five models, FeN_4-6r-c1 and FeN_4-6r-c2 possess lower ΔG of 0.31 and 0.32 eV, respectively (Figure 5c, Figure S27 and Table S7). But FeN_4-6r-c1 presents high resistance (0.72 eV) for the fifth step ($OH^* + e^- \rightarrow OH^-$), whereas for FeN_4-6r-c2 with higher cracking degree is more surmountable (0.13 eV). On the whole, defective FeN_4-6r-c2, located at the edge of voids, exhibits the lowest overall reaction free energy change (0.32 eV) (Table S8). Figure S28 illustrates edge-N atoms affect the distortion of Fe—N_4 as well as the intermediates adsorption configurations. These results reinforced that C—N structures altered the charge density distribution and electronic structures of active sites.

In summary, we reported the edge-site engineering of atomically dispersed, edge-hosted Fe—N_4 sites embedded in

DOI: 10.1021/jacs.8b07294
J. Am. Chem. Soc. 2018, 140, 11594−11598

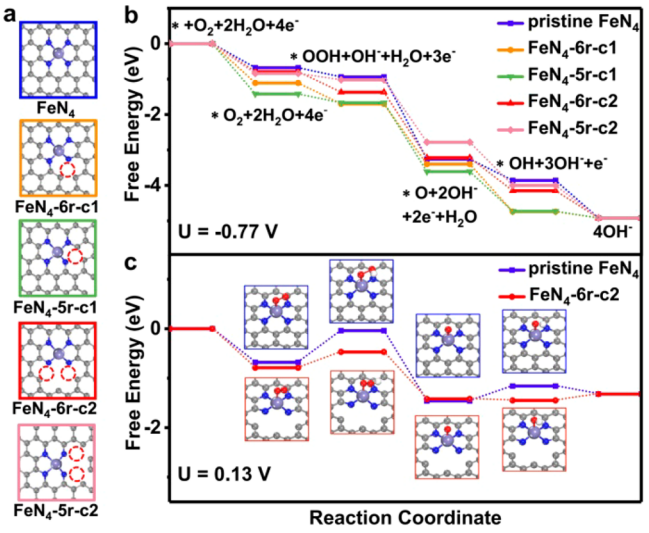

Figure 5. (a) Five possible atomic configurations with different cracking degree (6r or 5r refers to the six- or five-membered Fe—N-heterocyclic ring, respectively; c1 or c2 refers to the cleavage of one or two C—N bond adjacent to Fe—N_4, respectively). Free energy diagram (b) at $U = -0.77$ V, (c) at $U = 0.13$ V (vs SHE).

micro-mesoporous carbon. Both experiments and DFT calculations revealed that hierarchical pores triggered the selective C—N bond cleavage (SBC) neighboring Fe—N_4 sites. Such edge-hosted Fe—N_4 configuration is the key to tailoring the bonding structures of N, which remarkably decreases the overall ORR barriers. This work not only achieves the rational design and precise synthesis of single-atom catalyst but also provides in-depth understanding of active sites.

■ ASSOCIATED CONTENT

Supporting Information

The Supporting Information is available free of charge on the ACS Publications website at DOI: 10.1021/jacs.8b07294.

Experimental procedures, characterization methods, and additional figures and tables (PDF)

■ AUTHOR INFORMATION

Corresponding Authors

*chenyg@mail.buct.edu.cn

*lywang@mail.buct.edu.cn

ORCID

Tian Sheng: 0000-0001-5711-3012

Yueguang Chen: 0000-0002-3285-4938

Leyu Wang: 0000-0002-5961-7764

Notes

The authors declare no competing financial interest.

■ ACKNOWLEDGMENTS

This research was supported by the National Natural Science Foundation of China (21725501, 21475007, 21675009 and 21701005), the Fundamental Research Funds for the Central Universities (buctrc201812 and buctrc201815) and the China Postdoctoral Science Foundation (2017M620583). We also thank the support from the Public Hatching Platform for Recruited Talents of Beijing University of Chemical Technology.

■ REFERENCES

(1) Seh, Z. W.; Kibsgaard, J.; Dickens, C. F.; Chorkendorff, I.; Norskov, J. K.; Jaramillo, T. F. *Science* **2017**, *355*, eaad4998.

(2) Li, J.; Yin, H.-M.; Li, X.-B.; Okunishi, E.; Shen, Y.-L.; He, J.; Tang, Z.-K.; Wang, W.-X.; Yücelen, E.; Li, C.; Gong, Y.; Gu, L.; Miao, S.; Liu, L.-M.; Luo, J.; Ding, Y. *Nat. Energy* **2017**, *2*, 17111.

(3) Chen, L.; Lu, L.; Zhu, H.; Chen, Y.; Huang, Y.; Li, Y.; Wang, L. *Nat. Commun.* **2017**, *8*, 14136.

(4) Jiang, W. J.; Gu, L.; Li, L.; Zhang, Y.; Zhang, X.; Zhang, L. J.; Wang, J. Q.; Hu, J. S.; Wei, Z.; Wan, L. J. *J. Am. Chem. Soc.* **2016**, *138*, 3570.

(5) Huang, H.; Li, K.; Chen, Z.; Luo, L.; Gu, Y.; Zhang, D.; Ma, C.; Si, R.; Yang, J.; Peng, Z.; Zeng, J. *J. Am. Chem. Soc.* **2017**, *139*, 8152.

(6) Jackson, C.; Smith, G. T.; Inwood, D. W.; Leach, A. S.; Whalley, P. S.; Callisti, M.; Polcar, T.; Russell, A. E.; Levecque, P.; Kramer, D. *Nat. Commun.* **2017**, *8*, 15802.

(7) Bu, L.; Zhang, N.; Guo, S.; Zhang, X.; Li, J.; Yao, J.; Wu, T.; Lu, G.; Ma, J.-Y.; Su, D.; Huang, X. *Science* **2016**, *354*, 1410.

(8) Nie, Y.; Li, L.; Wei, Z. *Chem. Soc. Rev.* **2015**, *44*, 2168.

(9) Chen, D.; Chen, C.; Baiyee, Z. M.; Shao, Z.; Ciucci, F. *Chem. Rev.* **2015**, *115*, 9869.

(10) Li, Y.; Zhou, W.; Wang, H.; Xie, L.; Liang, Y.; Wei, F.; Idrobo, J. C.; Pennycook, S. J.; Dai, H. *Nat. Nanotechnol.* **2012**, *7*, 394.

(11) Zheng, Y.; Jiao, Y.; Zhu, Y.; Cai, Q.; Vasileff, A.; Li, L. H.; Han, Y.; Chen, Y.; Qiao, S. Z. *J. Am. Chem. Soc.* **2017**, *139*, 3336.

(12) Wang, B.; Wang, X.; Zou, J.; Yan, Y.; Xie, S.; Hu, G.; Li, Y.; Dong, A. *Nano Lett.* **2017**, *17*, 2003.

(13) Strickland, K.; Miner, E.; Jia, Q.; Tylus, U.; Ramaswamy, N.; Liang, W.; Sougrati, M.-T.; Jaouen, F.; Mukerjee, S. *Nat. Commun.* **2015**, *6*, 7343.

(14) Chen, Y.; Ji, S.; Chen, C.; Peng, Q.; Wang, D.; Li, Y. *Joule* **2018**, *2*, 1242.

(15) Wang, A.; Li, J.; Zhang, T. *Nat. Rev. Chemistry* **2018**, *2*, 65.

(16) Rogge, S. M. J.; Bavykina, A.; Hajek, J.; Garcia, H.; Olivos-Suarez, A. I.; Sepulveda-Escribano, A.; Vimont, A.; Clet, G.; Bazin, P.; Kapteijn, F.; Daturi, M.; Ramos-Fernandez, E. V.; Llabres i Xamena, F. X.; Van Speybroeck, V.; Gascon, J. *Chem. Soc. Rev.* **2017**, *46*, 3134.

(17) Zhang, H.; Liu, G.; Shi, L.; Ye, J. *Adv. Energy Mater.* **2018**, *8*, 1701343.

(18) Zhao, C.; Dai, X.; Yao, T.; Chen, W.; Wang, X.; Wang, J.; Yang, J.; Wei, S.; Wu, Y.; Li, Y. *J. Am. Chem. Soc.* **2017**, *139*, 8078.

(19) Liu, Z.; Sun, F.; Gu, L.; Chen, G.; Shang, T.; Liu, J.; Le, Z.; Li, X.; Wu, H. B.; Lu, Y. *Adv. Energy Mater.* **2017**, *7*, 1701154.

(20) Wang, Q.; Zhou, Z.-Y.; Lai, Y.-J.; You, Y.; Liu, J.-G.; Wu, X.-L.; Terefe, E.; Chen, C.; Song, L.; Rauf, M.; Tian, N.; Sun, S.-G. *J. Am. Chem. Soc.* **2014**, *136*, 10882.

(21) Chung, H. T.; Cullen, D. A.; Higgins, D.; Sneed, B. T.; Holby, E. F.; More, K. L.; Zelenay, P. *Science* **2017**, *357*, 479.

(22) Zhang, H.; Hwang, S.; Wang, M.; Feng, Z.; Karakalos, S.; Luo, L.; Qiao, Z.; Xie, X.; Wang, C.; Su, D.; Shao, Y.; Wu, G. *J. Am. Chem. Soc.* **2017**, *139*, 14143.

(23) Han, A.; Chen, W.; Zhang, S.; Zhang, M.; Han, Y.; Zhang, J.; Ji, S.; Zheng, L.; Wang, Y.; Gu, L.; Chen, C.; Peng, Q.; Wang, D.; Li, Y. *Adv. Mater.* **2018**, *30*, 1706508.

(24) Liang, H. W.; Bruller, S.; Dong, R.; Zhang, J.; Feng, X.; Mullen, K. *Nat. Commun.* **2015**, *6*, 7992.

(25) Yin, P.; Yao, T.; Wu, Y.; Zheng, L.; Lin, Y.; Liu, W.; Ju, H.; Zhu, J.; Hong, X.; Deng, Z.; Zhou, G.; Wei, S.; Li, Y. *Angew. Chem., Int. Ed.* **2016**, *55*, 10800.

(26) Armel, V.; Hindocha, S.; Salles, F.; Bennett, S.; Jones, D.; Jaouen, F. *J. Am. Chem. Soc.* **2017**, *139*, 453.

(27) Chen, Y.; Ji, S.; Wang, Y.; Dong, J.; Chen, W.; Li, Z.; Shen, R.; Zheng, L.; Zhuang, Z.; Wang, D.; Li, Y. *Angew. Chem., Int. Ed.* **2017**, *56*, 6937.

(28) Zhang, Z.; Chen, Y.; Xu, X.; Zhang, J.; Xiang, G.; He, W.; Wang, X. *Angew. Chem., Int. Ed.* **2014**, *53*, 429.

(29) Kramm, U. I.; Herrmann-Geppert, I.; Behrends, J.; Lips, K.; Fiechter, S.; Bogdanoff, P. *J. Am. Chem. Soc.* **2016**, *138*, 635.

DOI: 10.1021/jacs.8b07294
J. Am. Chem. Soc. 2018, 140, 11594−11598

(30) Fan, L.; Liu, P. F.; Yan, X.; Gu, L.; Yang, Z. Z.; Yang, H. G.; Qiu, S.; Yao, X. *Nat. Commun.* **2016**, *7*, 10667.
(31) Huang, P.; Lethien, C.; Pinaud, S.; Brousse, K.; Laloo, R.; Turq, V.; Respaud, M.; Demortiere, A.; Daffos, B.; Taberna, P. L.; Chaudret, B.; Gogotsi, Y.; Simon, P. *Science* **2016**, *351*, 691.
(32) Zhang, M.; Wang, Y. G.; Chen, W.; Dong, J.; Zheng, L.; Luo, J.; Wan, J.; Tian, S.; Cheong, W. C.; Wang, D.; Li, Y. *J. Am. Chem. Soc.* **2017**, *139*, 10976.
(33) Wu, G.; More, K. L.; Johnston, C. M.; Zelenay, P. *Science* **2011**, *332*, 443.
(34) Lu, Z.; Chen, G.; Siahrostami, S.; Chen, Z.; Liu, K.; Xie, J.; Liao, L.; Wu, T.; Lin, D.; Liu, Y.; Jaramillo, T. F.; Nørskov, J. K.; Cui, Y. *Nat. Catal.* **2018**, *1*, 156.
(35) Meng, J.; Niu, C.; Xu, L.; Li, J.; Liu, X.; Wang, X.; Wu, Y.; Xu, X.; Chen, W.; Li, Q.; Zhu, Z.; Zhao, D.; Mai, L. *J. Am. Chem. Soc.* **2017**, *139*, 8212.
(36) Sun, H.; Mei, L.; Liang, J.; Zhao, Z.; Lee, C.; Fei, H.; Ding, M.; Lau, J.; Li, M.; Wang, C.; Xu, X.; Hao, G.; Papandrea, B.; Shakir, I.; Dunn, B.; Huang, Y.; Duan, X. *Science* **2017**, *356*, 599.
(37) Tong, Y.; Chen, P.; Zhou, T.; Xu, K.; Chu, W.; Wu, C.; Xie, Y. *Angew. Chem., Int. Ed.* **2017**, *56*, 7121.
(38) Su, D. S.; Sun, G. *Angew. Chem., Int. Ed.* **2011**, *50*, 11570.
(39) Tan, H.; Li, Y.; Jiang, X.; Tang, J.; Wang, Z.; Qian, H.; Mei, P.; Malgras, V.; Bando, Y.; Yamauchi, Y. *Nano Energy* **2017**, *36*, 286.

DOI: 10.1021/jacs.8b07294
J. Am. Chem. Soc. 2018, 140, 11594−11598